AIAA JOURNAL
Vol. 43, No. 3, March 2005

Uncertainty Analysis of Laser-Doppler-Velocimetry Measurements in a Swirling Flowfield

Venkatraman A. Iyer* and Mark A. Woodmansee*
General Electric Global Research Center, Niskayuna, New York 12309

A statistical analysis of instantaneous laser-Doppler-velocimetry (LDV) measurements acquired in a swirling flowfield is performed. Instrument uncertainties associated with each velocity realization propagate into the ensemble statistics. Integral quantities such as the integrated mass flow rate and swirl number are susceptible to precision uncertainties associated with the instrument's optics, lasers, and electronics. In this study, experimental data are used in conjunction with an analytical model to determine the precision uncertainty of the first three velocity moments. With this analysis, the effects of ensemble size and probe volume location within the flowfield are accounted for. The statistical model is applied to LDV data acquired downstream of an aircraft engine combustor swirler. We show that the precision uncertainties associated with these swirler measurements bound the amount of information that can be extracted from the profiles.

Nomenclature

G_m = axial thrust, N
G_t = tangential thrust, N
K = kurtosis
k = turbulent kinetic energy, m^2/s^2
n = number of samples
r_s = split radius, m
S = skewness
S' = skewness including instrument uncertainty
U = axial velocity, m/s
W = tangential velocity, m/s
x = instantaneous laser-Doppler-velocimetry measurement
Δ = measurement error or bias
$\bar{\ }$ = mean value

Subscripts

i = ith instantaneous measurement
rms = rms value

Introduction

LASER Doppler velocimetry (LDV) is a nonintrusive technique employed by the combustion community to acquire spatially resolved gas-phase velocities in turbulent reacting flowfields. Interested readers are readily referred to Adrian[1] for a detailed description of the LDV technique.

In short, a pair of monochromatic laser beams (typically from an argon-ion laser) is focused to a point in the flow. The waists of the two beams are crossed, creating a fringe pattern at their intersection. Small seed particles introduced into the flow via fluidized bed or liquid atomizer pass through the fringe pattern and scatter the light via Mie scattering. Two filtered photodetectors and associated spherical lenses collect a portion of the scattered light for processing.

The frequency of the scattered light, often referred to as the Doppler frequency, is dependent upon the spacing of the fringes in the probe volume as well as the velocity of the entrained particle as it crosses the fringes' maxima and minima. Having a priori knowledge of the fringe spacing, the particle's velocity can be calculated. Similarly, knowing that the particle faithfully[2] follows the flowfield, instantaneous gas velocities can be deduced.

In practice, thousands of realizations are collected at each spatial location, allowing ensemble-based statistics such as the mean and rms velocities, to be calculated. In the swirler design community, LDV and other experimental techniques[3] are used to validate new swirler designs. Metrics[4] such as swirl number, split radius, mass flow rate, and recirculation zone strength are used to differentiate swirlers before their implementation into a combustor. Differences between swirlers are subtle, forcing the researcher to draw conclusions from near-inconclusive data.

To assist in these situations, this study estimates both the accuracy and precision of the instantaneous velocity measurements obtained using a two-color, dual-beam LDV system. A number of previous studies[5,6] have performed rms analyses of the individual optical/electronic/photonic components that comprise an LDV system. However, here we use a known velocity gauge to incorporate the uncertainties into a single scalar. Similarly, the uncertainties associated with the instantaneous velocity measurements are integrated into physically tractable parameters such as the velocity mean, rms, skewness, and kurtosis. Complementing this effort, the uncertainty of our translation system is estimated, allowing the addition of error bars to both the independent (probe volume position) and dependent (velocity) axes of the plots containing the swirler velocity profiles.

Previous studies on this topic have focused primarily on the statistical bias in the mean and rms velocities obtained from LDV measurements.[5,7,8] To the best of the authors' knowledge, the current study is the first to estimate uncertainties in higher-order statistics (rms and skewness) derived from these data as well as those found in swirling flowfields.

Equipment and Facilities

All work was carried out at the General Electric Global Research Center in Niskayuna, New York. Figure 1 is a schematic of the two-component TSI LDV instrument used to acquire the data for this study. The heart of the system is a Spectra Physics Stabilite 2017 5W argon-ion laser. The broadband laser is dispersed into two wavelengths: 514 nm (green) and 488 nm (blue), which are transported to the transceiver via multimode fiber-optic cable. The LDV transceiver emits the two beam pairs, where each pair is orthogonal to the other. The two fringe patterns at the point of intersection form the measurement volume. The setup is such that the green beams (defined as channel 1) measure the streamwise (or axial) velocity component U, and the blue beams (channel 2) measure the swirl

Presented as Paper 2004-1226 at the 42nd Aerospace Sciences Meeting, Reno, NV, 5–8 January 2004; received 18 February 2004; revision received 27 July 2004; accepted for publication 22 September 2004.

*Mechanical Engineer, Combustion Laboratory, Energy and Propulsion Technologies. Member AIAA.

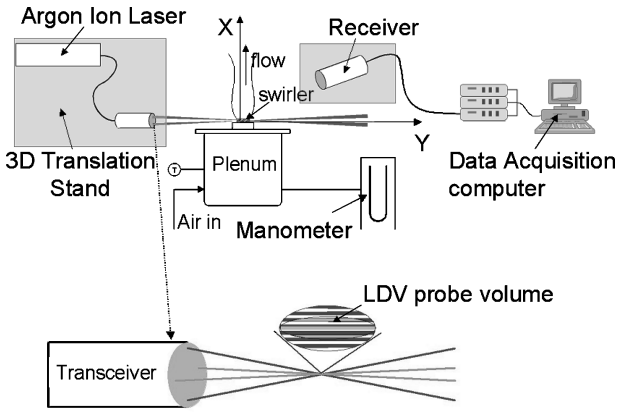

Fig. 1 Schematic of two-component LDV system.

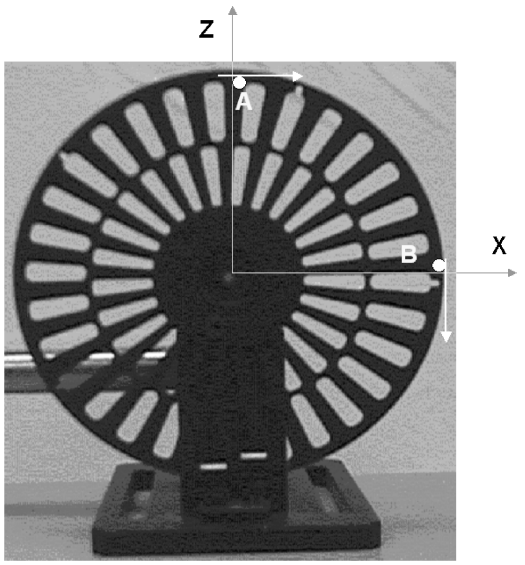

Fig. 2 Optical chopper for LDV system validation.

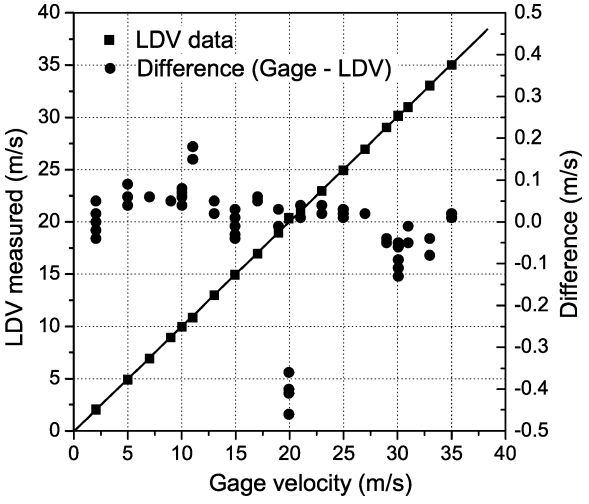

a) Channel 1

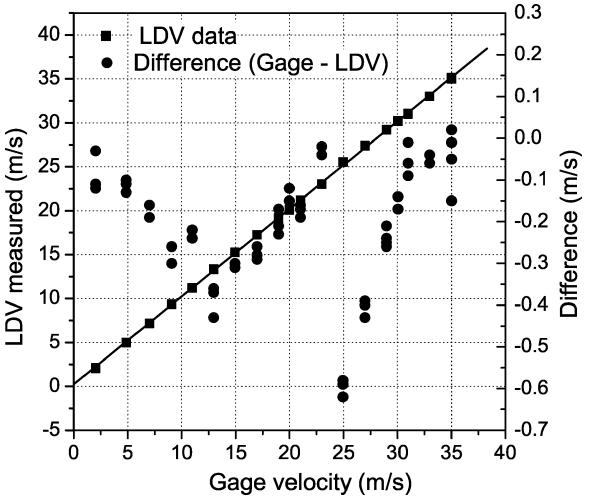

b) Channel 2

Fig. 3 Mean velocity.

(or azimuthal) velocity W downstream of the trailing edge of the swirler.

Uncertainty of Velocity Realizations

As just stated, the characterization of a turbulent flowfield using LDV involves the acquisition of hundreds or thousands of instantaneous velocity measurements at a fixed point in space. Prior work[5] investigated the uncertainties of the individual components that make up the entire instrument. However, in this study a direct approach is used to estimate the uncertainty in the LDV system by acquiring multiple measurements of a temporally steady gauge.

Here, an optical chopper wheel is used to generate the required known velocity. As shown in Fig. 2, the chopper wheel has 30 slots in its outermost ring. The wheel rotates at a specified angular velocity controlled by the operator. When the LDV probe volume is focused at the plane of the chopper wheel, the wheel's perforations move through the LDV fringes at a fixed linear velocity. This velocity is the linear distance from the axis of rotation multiplied by the angular velocity (in rad/sec) of the wheel. By controlling the rotational frequency of the wheel, a range of simulated particle velocities, from 5 to 35 m/s, can be explored.

By focusing the probe at the two points A and B as shown in Fig. 2, the velocity in channels 1 and 2 can be measured independently. At point A, the velocity of the slot will be in the horizontal direction, equal to the velocity measured in channel 1; at point B, the velocity will be in the vertical direction, equal to the velocity measured in channel 2. Figures 3a and 3b show the mean velocity of the LDV system as a function of the gauge velocity for channels 1 and 2, respectively. Each point in the figure is the average of an ensemble of about 2500 velocity samples, where each sample is defined as the velocity of a single shot of the chopper wheel as it passes through the probe volume.

A second curve has been added to the graph to illustrate the difference between the LDV and the gauge velocities. Ideally, the difference, $\Delta = \bar{x}_{\text{gauge}} - \bar{x}_{\text{LDV}}$, should be identically zero over the entire range of gauge velocities. The small nonzero values are caused by the uncertainties in the LDV measurements. For channel 1, a one-sample t test[9] on Δ vs zero yields a p value of 0.25, which is greater than the statistically significant limit of $p = 0.05$. This implies that there is no evidence that Δ is different from zero with 95% confidence level. So the difference between the LDV and the gauge velocity is not statistically significant.

For channel 2 shown in Fig. 3b, the difference data are biased toward values less than zero. Thus, the LDV system is consistently measuring a mean velocity that is greater than the gauge. A t test on the difference against zero yields a p value of 2×10^{-16}. Therefore, the difference between the LDV system and the gauge is statistically significant. The 95% confidence interval of the difference is $[-0.3 \text{ m/s} < \Delta < -0.1 \text{ m/s}]$ with a mean value of -0.2 m/s. When a constant value of 0.2 m/s is subtracted from the LDV mean of channel 2, the p value for the difference becomes 0.43, which implies that the LDV and the gauge are now statistically similar. This bias of 0.2 m/s is hence subtracted from the LDV measurements of channel 2.

Figures 4a and 4b present the rms velocity of channels 1 and 2, respectively. In this particular case, the rms velocity is a true measure of the instrument's precision because the gauge (chopper

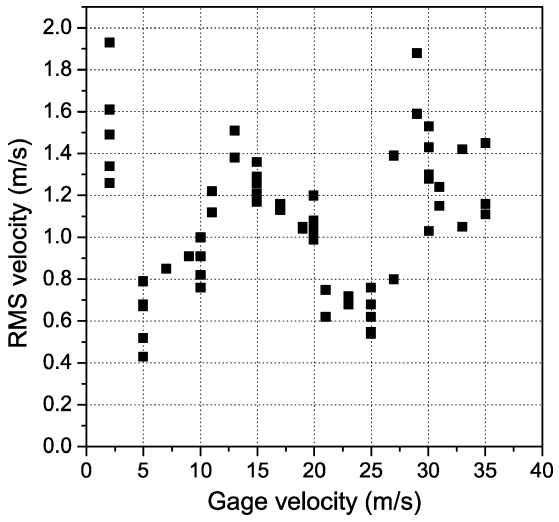

a) Channel 1

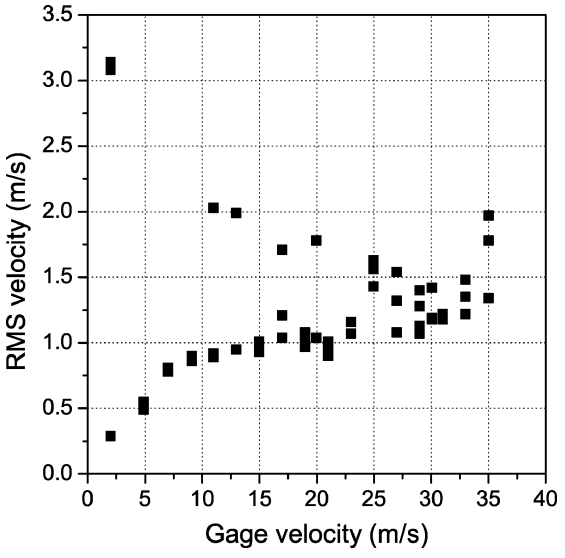

b) Channel 2

Fig. 4 RMS velocity.

wheel) is assumed to be perfectly steady. The chopper wheel has a frequency uncertainty of less than 2% of the instrument reading and a phase jitter of 0.5 deg. The figure shows that for both channels the standard deviation does not exhibit a coherent trend with respect to the gauge velocity. Therefore the precision of the LDV system is independent of the velocity being measured. Over the range of velocities examined, the standard deviation for channels 1 and 2 is estimated to be 1.08 and 1.22 m/s, respectively. These values are used in estimating the bias and variance of the statistical quantities discussed in the following two sections.

Figure 5 shows the skewness of the LDV system for channel 1 as a function of the gauge velocity. The positive skewness implies that the uncertainty in the LDV measurement is not normally distributed about the mean value but is skewed toward velocities greater than the mean. The skewness is higher for small velocities and decreases to a value of about five for large velocities. The continuous line shows the trend in the skewness as a function of the gauge velocity. Clearly, this skewness, which is inherent to the system, will influence the bias and uncertainty of the data acquired in the turbulent flowfield. Equally important, in our application the streamwise skewness is used to determine the radial split between two coswirling airstreams issuing from the inner and outer swirl vanes. The instrument's contribution to the skewness will affect the determination of the split radius. Because the skewness in channel 2 is not used in our data reduction, this parameter is not presented here.

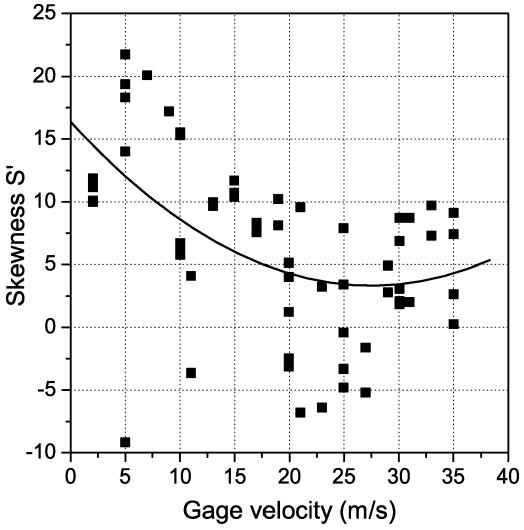

Fig. 5 Skewness.

Estimation of Bias

Bias is the deviation of the expected value of a statistical estimate from the quantity it estimates. The instrument's contribution to the bias of the collected data can be estimated using the uncertainty analysis of the instantaneous velocity measurements presented in the previous section. Clearly, this precision (or imprecision) of the LDV system should be presented when plotting different flowfield profiles and features. Here, the statistical quantities of interest are the mean velocity, rms velocity, and the skewness of the data acquired in the swirler flowfield.

Bias in Mean Velocity

The mean velocity of a sample of n particles is given by

$$\bar{x} = \sum_{i=1}^{n} x_i \Big/ n \tag{1}$$

where x_i is the instantaneous velocity measured for the ith particle. If there is a perturbation Δx_i in an individual velocity measurement x_i introduced by the instrument, then there will be an error $\Delta\bar{x}$ in the mean velocity as stated by

$$\bar{x} + \Delta\bar{x} = \sum_{i=1}^{n} (x_i + \Delta x_i) \Big/ n \tag{2}$$

Subtracting Eq. (2) from Eq. (1), we get

$$\Delta\bar{x} = \sum_{i=1}^{n} (\Delta x_i) \Big/ n \tag{3}$$

The right-hand side (RHS) of Eq. (3) is the mean deviation of the instantaneous LDV measurements from the true value as observed during the calibration process. Clearly, as n increases the effect of the instrument perturbation Δx_i is minimized. Moreover, if all of the LDV measurements are centered about the true value (as was observed during the calibration), then the bias in the mean velocity is zero.

Bias in rms of Velocity Fluctuations

The rms of velocity fluctuations in a turbulent flow is a measure of the variations in the individual fluctuations. For brevity, the term rms velocity is used to denote rms of the velocity fluctuations. For an LDV measurement of an ensemble of n particles, the rms velocity is defined as

$$x_{\text{rms}} = \left[\sum_{i=1}^{n} (x_i - \bar{x})^2 \Big/ (n-1) \right]^{\frac{1}{2}} \tag{4}$$

Perturbing the rms velocity in a manner consistent with the preceding mean velocity analysis, the bias in the rms velocity can be related to the perturbation of the instantaneous measurements by the following expression:

$$\Delta x_{\text{rms}} = \left[2 \sum_{i=1}^{n} \frac{(x_i - \bar{x})\Delta x_i}{n-1} + \sum_{i=1}^{n} \frac{(\Delta x_i)^2}{n-1} \right]^{\frac{1}{2}} \tag{5}$$

If the turbulence statistics are independent of the LDV error statistics, then the first summation on the RHS of Eq. (5) goes to zero because

$$\sum \Delta x_i = 0$$

The second summation on the RHS is the variance in the velocity measurements as a result of the LDV system σ^2. Thus the bias in x^2_{rms} is equal to the variance caused by the LDV system. The variance of the LDV system has to be subtracted from the measured mean square velocity fluctuations to get the expected value of x^2_{rms}:

$$x_{\text{rms}} = \sqrt{x'^2_{\text{rms}} - \sigma^2} \tag{6}$$

where x_{rms} and x'_{rms} are the expected and the measured values of the rms velocity, respectively.

Bias in Skewness

The skewness of the velocity distribution is defined as

$$S = \sum_{i=1}^{n} \frac{(x_i - \bar{x})^3}{(n-1)x^3_{\text{rms}}} \tag{7}$$

A positive skewness describes an ensemble of velocity realizations that, if plotted as a histogram, would have a longer "tail" toward higher velocities. When $S < 0$, then the histogram tail favors lower velocities. A skewness of zero represents a symmetric or balanced velocity histogram. In this study, the evolution[10] of the velocity skewness is used to locate boundary between two coflowing, coswirling freestreams.

The bias in the skewness as a result of the LDV system uncertainty can be estimated using the same procedure as for the mean and the rms velocities:

$$\Delta S = 3 \sum_{i=1}^{n} \frac{(x_i - \bar{x})^2 \Delta x_i}{(n-1)\, x^3_{\text{rms}}} + 3 \sum_{i=1}^{n} \frac{(x_i - \bar{x})\Delta x_i^2}{(n-1)\, x^3_{\text{rms}}} + \sum_{i=1}^{n} \frac{\Delta x_i^3}{(n-1)\, x^3_{\text{rms}}} \tag{8}$$

Assuming statistical independence between the turbulence and the LDV system, the first two summations on the RHS of Eq. (8) can be expressed as a product of summations that go to zero because

$$\sum \Delta x_i = 0, \qquad \sum (x_i - \bar{x}) = 0$$

The third summation on the RHS of Eq. (8) can be expressed as

$$\sum_{i=1}^{n} \frac{\Delta x_i^3}{(n-1)x^3_{\text{rms}}} = \left[\sum_{i=1}^{n} \frac{\Delta x_i^3}{(n-1)\sigma^3} \right] \left(\frac{\sigma}{x_{\text{rms}}} \right)^3 = S' \left(\frac{\sigma}{x_{\text{rms}}} \right)^3 \tag{9}$$

where S' is the skewness attributed to the LDV system, as estimated from Fig. 5. With these data, it is clear that the LDV system will influence the skewness acquired in the swirler flowfield. Knowing this, the instrument bias should be subtracted from the measured skewness to obtain the expected skewness value:

$$S_{\text{expected}} = S_{\text{measured}} - S'(\sigma / x_{\text{rms}})^3 \tag{10}$$

Estimation of Variance

Here, the principle of propagation of errors[11] is used to quantify the variance in statistical quantities derived from instantaneous measurements. If x_i represent i independent measurements and if y is related to them by the relation $y = f(x_i)$, then the variance in y, represented as σ_y^2, is related to the variance in the independent measurements $\sigma^2_{x_i}$ by the following expression:

$$\sigma_y^2 = \sum_{i=1}^{n} \left(\frac{\partial f}{\partial x_i} \right)^2 \sigma^2_{x_i} \tag{11}$$

If $\sigma^2_{x_i}$ is independent of x_i (as was evident in the preceding LDV uncertainty analysis), then by replacing $\sigma^2_{x_i}$ with σ^2, Eq. (11) reduces to

$$\sigma_y^2 = \sigma^2 \sum_{i=1}^{n} \left(\frac{\partial f}{\partial x_i} \right)^2 \tag{12}$$

Using Eq. (12), the variance associated with the mean, rms, and skewness scalars can be estimated. The application of this principle is presented next.

Variance of the Mean Velocity

The mean of n velocity measurements is given by Eq. (1). Applying Eq. (12) to Eq. (1), the variance of the mean velocity is given by

$$\sigma^2_{\bar{x}} = \sigma^2 \sum_{i=1}^{n} \left(\frac{1}{n} \right)^2 = \frac{\sigma^2}{n} \tag{13}$$

According to Eq. (13), the uncertainty in the mean velocity diminishes as the sample size n increases. Therefore, the influence of stochastic noise introduced by the LDV system can be minimized by increasing n.

Variance of the rms Velocity

The rms velocity can be rewritten as

$$x^2_{\text{rms}} = \sum_{i=1}^{n} \frac{(x_i - \bar{x})^2}{n-1} = \sum_{i=1}^{n} \frac{x_i^2 - \bar{x}^2}{n-1} \tag{14}$$

Using propagation of errors, Eq. (12), the variance in the rms velocity is given by

$$\sigma^2_{x^2_{\text{rms}}} = \sum_{i=1}^{n} \frac{4x_i^2\sigma^2}{(n-1)^2} + \left(\frac{n}{n-1} \right)^2 \sigma^2_{\bar{x}^2} \tag{15}$$

Simplifying Eq. (15) with some algebraic manipulations, the variance of the rms velocity for $n \to \infty$ becomes

$$\sigma^2_{x_{\text{rms}}} = \frac{\sigma^2}{n-1} \left[1 + \left(\frac{\bar{x}}{x_{\text{rms}}} \right)^2 \right] \tag{16}$$

From Eq. (16), the variance in the rms velocity decreases as the sample size is increased. Note that $\sigma^2_{x_{\text{rms}}}$ also depends on mean velocity $\bar{x}$. Interestingly, $\sigma^2_{x_{\text{rms}}}$ increases as velocity maxima or minima are approached.

Variance of the Skewness

Applying Eq. (12) to Eq. (7) and with a significant amount of algebraic manipulation, the variance in the skewness S for large values of n can be expressed as

$$\sigma_S^2 = 9 \left[\frac{\sigma}{x_{\text{rms}}\,(n-1)} \right]^2 \left[4S \frac{\bar{x}}{x_{\text{rms}}} + 6 \left(\frac{\bar{x}}{x_{\text{rms}}} \right)^2 + 2 \left(\frac{\bar{x}}{x_{\text{rms}}} \right)^4 + K + 4 \right] + 9 \left(\frac{\sigma_{x_{\text{rms}}}}{x_{\text{rms}}} \right)^2 \left[S^2 + 4 \left(\frac{\bar{x}}{x_{\text{rms}}} \right)^2 \right] \tag{17}$$

where K is the kurtosis[9] given by

$$K = \frac{1}{n-1}\sum_{i=1}^{n}\left(\frac{x_i - \bar{x}}{x_{\text{rms}}}\right)^4 - 3 \tag{18}$$

Again Eq. (17) is valid for large n. Similar to the variance in the mean and rms, the variance in skewness decreases with increasing sample size. Equally important, both $\bar{x}$ and $\sigma_{x_{\text{rms}}}$ play an integral role in determining σ_S^2. Regions of the flowfield where the mean and rms velocities are high will be subject to elevated levels of uncertainty in the velocity skewness.

Estimation of Spatial Uncertainty

The LDV positioning system, composed of three linear translations stages, also plays a role in the uncertainty of the velocity profiles. In our system, the LDV transceiver and receiver move in tandem; the alignment of these optic does not change regardless of the X, Y, or Z position. The translation stages are mounted orthogonally such that the table and hardware can move to any location within the limits of the stage.

The spatial uncertainty of the translation stage and position-feedback system is estimated by calibrating the translation stage against a machinist's dial indicator with a precision of 12 μm. For this study, the calibration is performed for the Y-translation stage because the system is moved in only one direction (radially) across the trailing edge of the swirler. As the table is translated, position measurements from the dial indicator and stage readout are recorded.

Figure 6 is a plot of the stage readout multimeter reading for different dial gauge readings. Also shown in Fig. 6 is the difference of the dial gauge and the stage readout over a range of 1.27 cm. Hysteresis in the stage readout is apparent as the stage is moved away from then toward the origin. The difference is predominantly negative when the stage is translated in the positive Y direction and positive when the stage is moved in the negative Y direction.

Assuming that the dial indicator is the accurate gauge, a one-sample t test of the difference against zero yields a p value of 0.3, which implies that the bias in the stage's position is not statistically significant. From this analysis, it can be concluded that the position of the translation stage is "accurate." The standard deviation of the difference between the stage and the dial indicator is approximately 106 μm. These data will be used as an estimation of the precision uncertainty of the LDV probe volume position in the following plots.

Application to Swirler Flowfield Measurements

Figure 7 is a schematic of the swirler flowfield; only half of the flowfield is plotted. The flow exiting the swirl vanes is split by a venturi into a primary and secondary streams. The primary stream flows through the inner region of the swirler where the fuel is normally introduced. The two streams come into contact at the exit or trailing edge of the venturi, creating a region of high turbulent kinetic energy (TKE) that aids in fuel air mixing. The swirling flow is strong enough to create a vortex breakdown,[4] generating a central toroidal recirculation zone at the trailing edge of the venturi. The central recirculation zone is responsible for stabilizing the diffusion flame in the engine. The strength of this recirculation zone is proportional to the magnitude of the swirl velocity. There is also a secondary recirculation zone above the venturi in the secondary stream as the flow separates and expands at the exit of the swirl vanes.

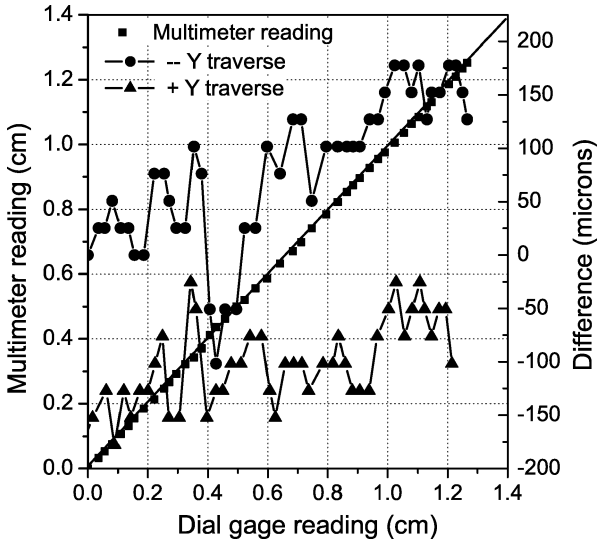

Fig. 6 Translation stage calibration.

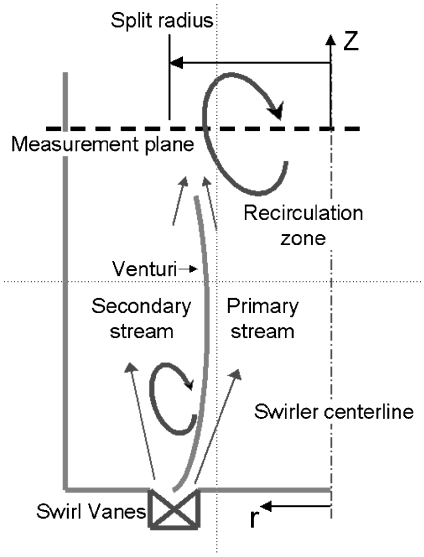

Fig. 7 Schematic of the swirler flowfield.

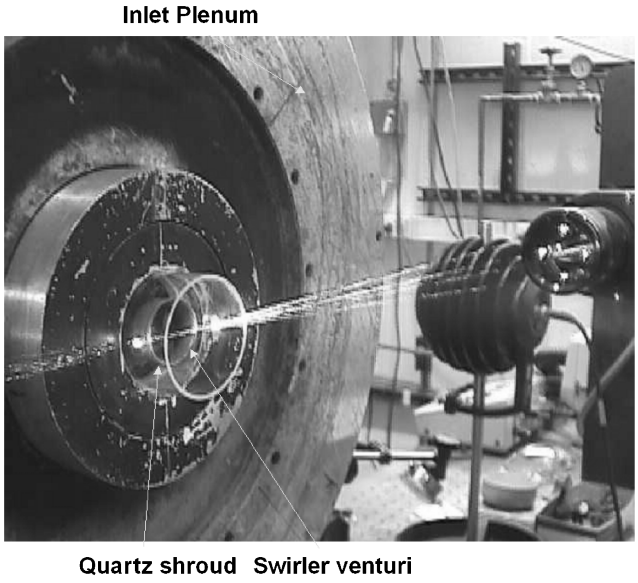

Fig. 8 Photograph of the swirler test stand.

Here, the LDV measurements are acquired to characterize this recirculation zone, which play a crucial role in determining the operability of the engine. All of the LDV measurements are taken at a plane downstream of the tip of the venturi as shown in Fig. 7. The flow is seeded with 0.1-μm TiO_2 particles.

Figure 8 presents a photograph of the swirler flow stand. A cylindrical quartz shroud (tube) is used to confine the flow exiting the venturi and to simulate physical boundaries found in the engine proper. Using the translation system, the LDV probe volume is traversed across the trailing edge of the swirler, providing U and W

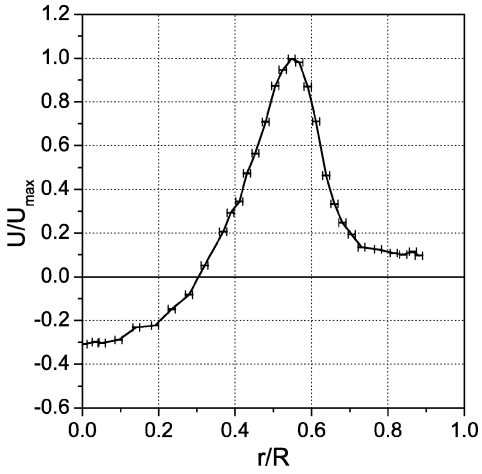

Fig. 9 Mean axial velocity.

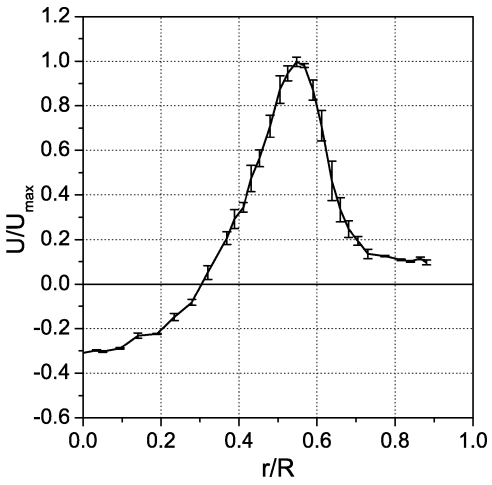

Fig. 10 Mean axial velocity. The total uncertainty includes the variation in the translation system.

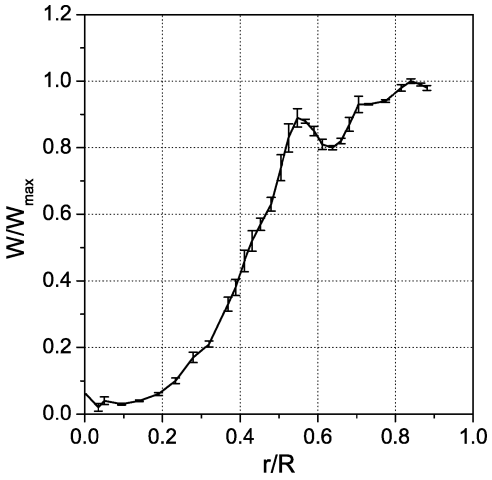

Fig. 11 Mean swirl velocity.

velocity profiles as a function of radial position. Each ensemble consists of 600–1000 realizations. Using Eqs. (1) and (4), respectively, the mean and the rms velocities are calculated from the data ensemble via the TSI software for each radial position.

Measurements of the Mean Velocity

Figure 9 is a plot of the mean streamwise velocity as a function of the radial location from the centerline ($r/R = 0$). The outer boundary of the recirculation zone ($U < 0$) reaches $r/R \approx 0.3$, where R is the radius of the quartz shroud. The maximum streamwise velocity $U_{\max}$ occurs at $r/R = 0.55$ and then decreases to $1/10\ U_{\max}$ at the outer boundary in the secondary flow. The error bars in Fig. 9 represent 95% confidence limits obtained from the variance in the mean velocity as given by Eq. (13). Also shown are the 95% confidence limits on the radial location of the probe as estimated from the uncertainty analysis of the positioning system. The uncertainty in the mean velocity is approximately 0.2% of $U_{\max}$. Correspondingly, the vertically oriented error bars are not visible in Fig. 9. The work of Herrin[5] estimated the uncertainty in the mean velocity to be 1.2% by propagating the worst-case uncertainties in the LDV optics to the estimated mean velocity. Because that approach was based on a worst-case scenario, the estimated uncertainties were greater than our estimate based on a top-down approach.

At a given radial location, the uncertainty of the probe-volume position adds to the uncertainty in the mean velocity. Therefore, using the following expression the total variance of the mean velocity can be expressed as the sum of the variances as a result of the LDV instrument and the positioning system

$$\sigma^2_{U_{\text{total}}} = \sigma^2_{U_{\text{LDV}}} + \left(\frac{\partial U}{\partial r}\right)^2 \sigma_r^2 \tag{19}$$

Figure 10 shows the total confidence limits on the mean axial velocity calculated from Eq. (19). As expected, the magnitude of the error bars grows in regions of high-velocity gradients. The maximum uncertainty in the peak regions is 8% of $U_{\max}$. The uncertainties in the mean velocity are dominated by precision errors in the positioning of the probe rather than the LDV system itself.

Figure 11 shows the mean swirl velocity as a function of the radial location. Because the swirl velocity is measured in channel 2, the instrument bias of 0.2 m/s as explained earlier is subtracted from the measured mean velocity. The swirl is close to zero at the centerline increases to about 90% of the maximum at $r/R = 0.55$ after which it slightly decreases and then again rises to the maximum in the secondary stream. This bimodal profile is typical of a two-stream swirl profile.[10] The error bars shown are calculated from the total variance inherent to the LDV instrument and the positioning system. Similar to the axial-velocity profiles, the uncertainties in the swirl-velocity distribution are dominated by the positioning system. The maximum uncertainty is of the order of 5% of $W_{\max}$.

Velocity Bias Correction for the Mean Velocity

In turbulent flowfields, the correlation between the fluid velocity and the particle seeding density can result in a bias of the mean velocity toward higher values.[5,8] Particles with higher velocities convect through the probe volume at a higher rate and will be detected more often than particles with lower velocities. The chopper-wheel calibration process is not intended to capture this bias because it is based on a constant angular velocity (rotation). Different methods for correcting for the velocity bias have been suggested in the literature.[8] One common method is to weight the individual velocities with the interarrival time between data realizations so that lower velocity particles that arrive slowly are weighted more.[8]

Figure 12 shows the unweighted mean axial velocity as a function of the radial location compared with the arrival-time weighted mean velocity for six different radial locations as shown by the square symbols in the figure. The difference between the weighted (unbiased) and the unweighted (biased) means are less than 2% of the maximum velocity and are certainly within the total uncertainty of the measurement system. It can be concluded that the velocity bias does not affect our measurements and will not be considered further. However, the uncertainty analysis presented here is applicable to flowfields where the velocity bias is important.

Measurements of the rms Velocity

The measured rms velocity consists of fluctuations both from the turbulent flowfield and the uncertainties in the LDV measurement. The rms velocity can be corrected for the instrument bias with Eq. (5). The error bars on the rms velocity are obtained from

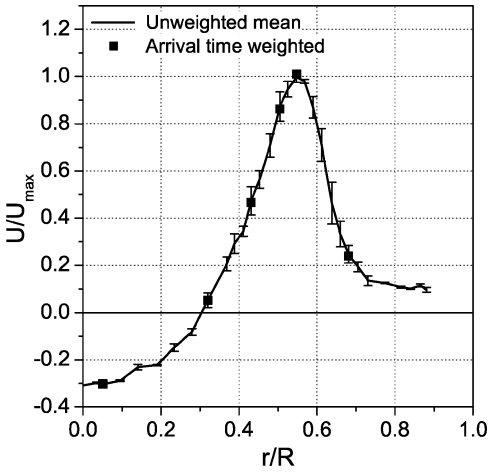

Fig. 12 Mean axial velocity. Comparison between unweighted and arrival-time weighted mean velocity.

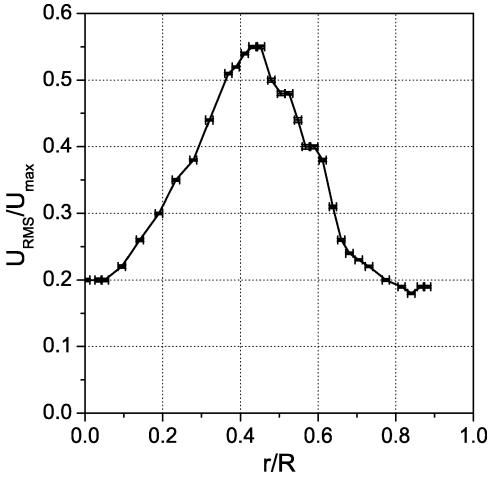

Fig. 13 RMS axial velocity.

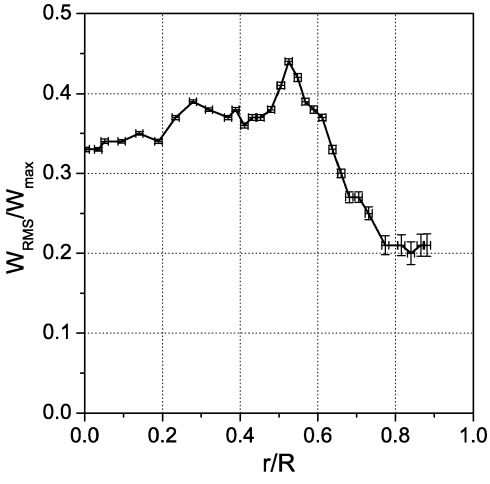

Fig. 14 RMS swirl velocity.

Eq. (16). Figure 13 shows the corrected rms of the axial velocity as a function of the radial coordinate. Again, as in Fig. 9, the position uncertainty dominates the instrument uncertainty. The rms velocity reaches a maximum at $r/R = 0.45$, radially inward of the mean axial velocity peak at $r/R = 0.55$. The 95% confidence limits on the axial rms velocity as a result of the LDV system are approximately 0.4% $U_{\max}$.

To complete this analysis, Fig. 14 presents W_{rms} as a function of the radius. The rms swirl velocity embodies two subtle peaks. There is a dominant peak at $r/R = 0.55$ and a less dominant one

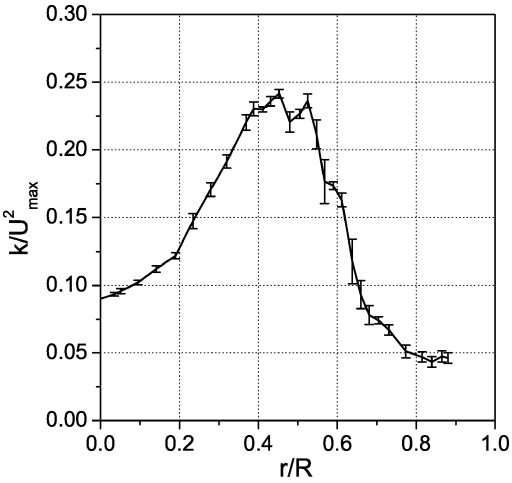

Fig. 15 Turbulent kinetic energy.

at $r/R = 0.3$. The precision uncertainty associated with the LDV system comprises 0.5% $W_{\max}$ with 95% confidence. However, the finite horizontal error bars in Fig. 14 show the uncertainty in the radial position is still a dominant feature.

The TKE can be calculated from the axial and swirl rms velocity data. Per previous efforts,[4] it is assumed that the rms of the radial velocity is identical to the swirl rms velocity. Applying this assumption, the turbulent kinetic energy k is defined as

$$k = \tfrac{1}{2}\left(U_{\text{rms}}^2 + 2W_{\text{rms}}^2\right) \tag{20}$$

The variance in the turbulent kinetic energy σ_k^2 can then expressed as

$$\sigma_k^2 = U_{\text{rms}}^2\sigma_{U_{\text{rms}}}^2 + 4W_{\text{rms}}^2\sigma_{W_{\text{rms}}}^2 \tag{21}$$

Figure 15 presents the turbulent kinetic energy k normalized by the square of the maximum axial velocity. The error bars are 95% confidence limits obtained from the variance calculated from Eq. (21). The maximum uncertainty in the turbulent kinetic energy is of the order of 15% $k/U_{\max}^2$.

Measurement of Skewness and Estimation of Split Radius

The radial location of the boundary between the primary and the secondary flows, referred to as the split radius, is an important metric for determining the variation in the recirculation zone size for different swirlers. Here, the split radius, is used as an integration limit for calculation of the primary and secondary swirl numbers. The strength of the swirl in these two zones ultimately controls the stability characteristics of the combustor flame. The split radius is determined from the streamwise skewness in the same manner as in Woodmansee et al.[10]

For a mixing layer of two streams with different velocities, the turbulent velocity distribution will be skewed to the left ($S < 0$) in the high-velocity side (primary stream) and to the right ($S > 0$) on the low-velocity side (secondary stream). As the probe volume transitions from the high- to low-velocity streams, S will transition from negative to positive values. At the zero crossing ($S = 0$), the streamwise velocity histogram is bimodal and symmetric. The zero crossing defines the spatial boundary between the two streams.

Figure 16 presents the skewness of the LDV measurements as a function of the radius. Applying Eq. (8), the skewness is corrected for the LDV system bias. The figure shows that between r/R of 0.55 and 0.65 the skewness changes from negative to positive when transitioning from the primary high-velocity stream to the secondary low-velocity stream. Thus, the split radius is $r_s/R = 0.6$ for this swirler.

The variance in the split radius is the sum of the contributions from the variance in the positioning system and the variance in the skewness as given by the following equation:

$$\sigma_{r_s}^2 = \sigma_r^2 + \frac{\sigma_{s(r=r_s)}^2}{(\partial S/\partial r)^2/r = r_s} \tag{22}$$

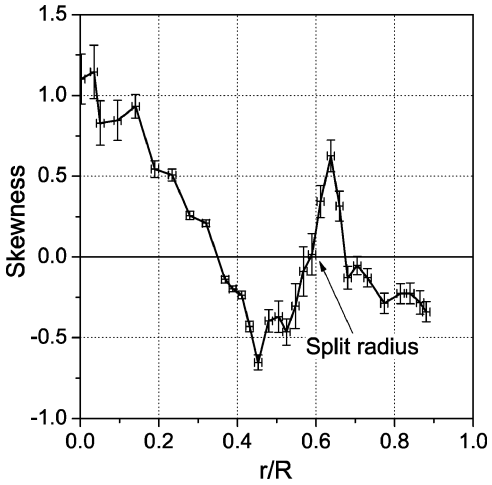

Fig. 16 Skewness in axial velocity.

The error bars, depicting the 95% confidence level of S in Fig. 16, are determined from Eq. (17). Unlike the mean and the rms velocities, the variance in the skewness caused by the LDV system appears to be more significant. This result is expected because skewness is a higher statistical moment and is therefore more sensitive to uncertainties than the mean and rms velocities. At the split location the 95% confidence interval in the skewness is about ± 0.13. Combining this value with the variance in the radial positioning system, the variance in the split radius is obtained from Eq. (22). The measurement of the split radius will be more precise if the gradient in the skewness going though the zero crossing is sharper. For the swirler under consideration, the normalized split radius is $r/R = 0.6 \pm 0.016$ with a 95% confidence interval.

Calculation of the Primary Swirl Number and Its Variance

The primary swirl number is an important parameter that characterizes the ability of the swirler to stabilize a flame in a swirling flow. According to Gupta et al.,[4] a swirling jet with a swirl number greater than 0.6 creates a recirculation zone at the center of the jet that helps stabilize the flame in the combustor. The primary swirl number S_p is defined as[10]

$$S_p = G_t/(r_s G_m) \tag{23}$$

where G_t and G_m are the tangential and axial thrusts, respectively, given by

$$G_t = \int_0^{r_s} 2\pi^2 r^2 \rho U W \, \mathrm{d}r, \qquad G_m = \int_0^{r_s} 2\pi^2 r_s \rho U^2 \, \mathrm{d}r \tag{24}$$

The primary swirl number is a flow invariant,[4] so that the streamwise plane of acquisition is not important. The primary swirl number, calculated from the velocity profiles in Figs. 10 and 11, is greater than 0.6, which is desirable for flame stabilization. The variance in the swirl number is obtained by applying Eq. (11) to Eq. (23):

$$\sigma_{S_p}^2 = S_p^2 \left(\frac{\sigma_{G_t}^2}{G_t^2} + \frac{\sigma_{G_m}^2}{G_m^2} + \frac{\sigma_{r_s}^2}{r_s^2} \right) \tag{25}$$

The variances in the axial and the tangential thrusts are calculated by summing the contributions caused by the uncertainties in the mean axial and tangential velocity at each radial location. Using the method just described, the 95% confidence in the swirl number is calculated to be ± 0.031. Thus, the swirl number can be estimated with a precision of $\pm 5\%$.

Summary

This paper presents a method to estimate instrument and position uncertainty of instantaneous laser-Doppler-velocimetry (LDV) velocity realizations. An optical chopper is used to provide a steady velocity gauge for the calibration of the LDV system. The uncertainty in the laser positioning system is also estimated using a dial indicator as a gauge. The uncertainties in the instantaneous measurements are then integrated into bias and variance calculations for the mean, rms, and skewness parameters. The propagation of variances is heavily relied upon to integrate the basic instrument uncertainties into the more complex swirl number and thrust calculations.

The uncertainty analysis is then applied to measurement acquired downstream of an aircraft engine swirler. Error estimates are obtained for the primary/secondary split radius and the primary swirl number. This process is very useful for comparing the integrated measurements between different (or similar) swirlers and providing insight on whether the differences in the velocity data are caused by part-to-part variations or uncertainties associated with the instrument.

References

[1] Adrian, R. J., "Laser Velocimetry," *Fluid Mechanics Measurements*, 2nd ed., edited by R. J. Goldstein, Taylor and Francis, Washington, DC, 1996, pp. 175–293.

[2] Samimy, M., and Lele, S. K., "Motion of Particles with Inertia in a Compressible Free Shear Layer," *Physics of Fluids: A*, Vol. 3, No. 8, 1991, pp. 1915–1923.

[3] Lefebvre, A. H., *Atomization and Sprays*, Hemisphere, New York, 1989, pp. 367–409.

[4] Gupta, A. K., Lilliey, D. G., and Syred, N., *Swirl Flows*, Abacus Press, Kent, England, U.K., 1984, Chap. 1.

[5] Herrin, J. L., "An Experimental Investigation of Supersonic Axisymmetric Base Flow Including the Effects of Afterbody Boattailing," Ph.D. Dissertation, Dept. of Mechanical and Industrial Engineering, Univ. of Illinois, Urbana, IL, July 1993.

[6] Resagk, C., du Puits, R., and Thess, A., "Error Estimation of Laser-Doppler Anemometry Measurements in Fluids with Spatial Inhomogeneities of the Refractive Index," *Experiments in Fluids*, Vol. 35, No. 4, 2003, pp. 357–363.

[7] Edwards, R. V., "Report on the Special Panel on Statistical Particle Bias Problems in Laser Anemometry," *Journal of Fluids Engineering*, Vol. 109, No. 2, 1987, pp. 89–93.

[8] Hoesel, W., and Rodi, W., "New Biasing Elimination Method for Laser-Doppler Velocimeter Counter Processing," *Review of Scientific Instruments*, Vol. 48, No. 7, 1977, pp. 910–919.

[9] Hogg, R. V., and Tanis, E. A., *Probability and Statistical Inference*, Macmillan, New York, 1993, p. 299.

[10] Woodmansee, M. A., Ball, I. C., and Barlow, K. W., "Experimental Flowfield Characterization of a Combustor Swirl Cup," AIAA Paper 2002-2864, June 2002.

[11] Kline, S. J., and McClintock, F. A., "Describing Uncertainties in Single-Sample Experiments," *Mechanical Engineering*, Vol. 75, No. 1, 1953, pp. 3–8.

J. Trolinger
Guest Editor